**Title:**

# NADH biofluoro-shifting to red light toward multi-wavelength imaging application of VOCs


**Authors and affiliation**

Kenta Iitani[a], Rintaro Miura[b], Jifu Lim[b], Kenta Ichikawa[a], Koji Toma[c], Kohji Mitsubayashi[a, b, *]

[a] *Department of Biomedical Devices and Instrumentation, Institute of Biomaterials and Bioengineering, Tokyo Medical and Dental University, 2-3-10 Kanda-Surugadai, Chiyoda-ku, Tokyo 101-0062, Japan*

[b] *Graduate School of Medical and Dental Sciences, Tokyo Medical and Dental University, 1-5-45 Yushima, Bunkyo-ku, Tokyo 113-8510, Japan*

[c] *College of Engineering, Shibaura Institute of Technology, 3-7-5 Toyosu, Koto-ku, Tokyo 135-8548, Japan*

***Corresponding author:**

*K. Mitsubayashi, Tel.: +81 3 5280 8091, Fax: +81 3 5280 8094, E-mail: m.bdi@tmd.ac.jp*

**Abstract**

In breath and transdermal gas, which contain thousands of volatile organic compounds (VOCs), selective simultaneous measurement of multiple VOCs is considered effective for noninvasive pharmacokinetic and metabolic tracking. Enzymatic optical biosensors with high selectivity and sensitivity have potential for simultaneous sensing and imaging of multiple VOCs by wavelength discrimination, but most enzymatic optical biosensors emit blue light region (400–500 nm). In this study, we investigated the possibility of red shifting the wavelength of luminol chemiluminescence (CL) and NADH fluorescence (FL), which emits blue light, for multiplexed VOCs imaging. Luminol CL and NADH FL were converted to red by addition of rhodamine B and by resorufin (excitation 560 nm, fluorescence 590 nm) which induced by diaphorase (DP) with resazurin. The results showed that resorufin was suitable for multiplexing because the spectrum overlap with blue region was minimal. In addition, a DP-immobilized cotton mesh enabled spatiotemporal imaging of NADH mist spray at optimal of various conditions (buffer pH = 6.5, DP amount = 60 U/cm$^2$, initial resazurin = 100 μM) with fast response (90% response time = 10 s). Furthermore, the NADH detection sensitivity was sufficient for VOCs imaging with red light in combination with NADH-dependent enzymes. In the future, this technique can be used for simultaneous imaging of multiple VOCs in the same region of interest.

**Keywords:**

Image sensing, NADH, resorufin, diaphorase, biosensor, immobilization

## Introduction

Assessment of metabolic function and disease diagnosis typically involve blood samples that require invasive collection. On the other hand, exhaled breath and transdermal gases can be collected noninvasively.[1,2] Therefore, they can be used for high-frequently medical check-up or health monitoring. Those exhaled breath and transdermal gases contain blood-borne volatile organic compounds (VOCs).[3,4] Since some of them are produced or removed by internal metabolism, they can be used to monitor biochemical status.[5–7] If VOCs in breath and transdermal gases can be easily measured and longitudinal VOCs changing profiles can be accumulated, it may be possible to detect metabolic abnormalities caused by diseases and infections from changes in VOCs concentrations. It was reported that nearly 1,500 different trace concentration of VOCs are contained in exhaled breath.[8] This means that highly selective and sensitive system is required for human-borne VOCs measurement. At the basic research level, analytical systems with high sensitivity and high selectivity, such as gas chromatography-mass spectrometry, are used.[9,10] However, it is impossible to utilize these analytical systems for healthy people on daily basis. Therefore, development various types of easy-to-use gas sensors that are small enough to be owned by individuals is under way.[11–21]

Currently, many gas sensors face the challenge of selectivity. To address this challenge, we are developing gas sensors that focus on the molecular recognition ability of enzymes.[22,23] The enzyme is suitable for human-borne VOC sensors that require selectivity because of its substrate specificity. Furthermore, the use of light for quantification of enzymatic reactions enables highly sensitive measurement.

One of the advantages of using light as a measurement medium is that distributions (spatial information) can be easily obtained.[24,25] If there is a mechanism for light intensity to vary with VOCs concentration in space, the spatiotemporal distribution of VOCs concentrations can be evaluated.[26,27] Another advantage is that specific wavelengths can be easily isolated to

measure based on multiband or hyperspectral imaging technique.[28,29] In principle, it is possible to respond to different VOCs at different wavelengths and simultaneously measure multiple VOCs in the same space, which allowed to monitoring the metabolic kinetics of pharmaceuticals and tracking multiple VOCs associated with diseases noninvasively. The utility of optical measurement for simultaneous measurement of multiple substances is well known in molecular biology. For instance, Chen *et al.* used excitation spectral microscopy to achieve simultaneous imaging of 10 different fluorophores with less than 0.5 % of cross-talk.[30] Using this method, one can simultaneously measure the distribution of 10 different molecules, proteins, organelles, and etc. labeled with different fluorophores.

On the other hand, label-free enzyme-based optical biosensors, which are easily deployed for continuous measurement, are limited in the wavelengths-bands they can use. For example, chemiluminescence (CL) produced by the luminol-horse radish peroxidase (HRP) system and autofluorescence (FL) of reduced nicotinamide adenine dinucleotide (NADH) are commonly used in label-free enzyme-based optical biosensors.[31] The wavelength of these lights almost overlap at 400–500 nm. While probes that can convert the wavelength of NADH FL have been developed,[32–34] their accessibility is limited because most of them must be synthesized on their own. This has been a challenge to realize multiplexed enzyme biosensors by using different wavelength of light in the same space.

A method for measuring NADH concentration by fluorescence at red region (500–600 nm) has been used by using diaphorase (DP), which reduce resazurin with NADH as a substrate to resorufin with its fluorescence (ex 560 nm, fl 590 nm).[35,36] Another known method is to mix fluorophore in the luminol CL reaction solution and change the emission color by energy transfer.[37,38] However, with best of our knowledge, attempts at macroscopic chemical imaging using these simple light color changing methods are lacking. In this study, we compared luminol CL + fluorophore and NADH-DP-resazurin system for multiplexing with blue-colored light. In

addition, quantitative chemical imaging applicable to enzymatic optical biosensors was discussed using a method suitable for multi-wavelength imaging of VOCs.

## Experimental methods

### Reagents

HRP (product# 169-10791, >100 U/mg) was purchased from FUJIFILM Wako Chemicals, Japan. DP (product# 46446003, from *Clostridium Kluyveri*, 181 U/mg powder) was purchased from Oriental Yeast, Japan. Glutaraldehyde (GA, 25%, product# 079-00533) was from FUJIFILM Wako Chemicals. Hydrogen peroxide (30.0–35.5%, product# 18084-00) was from Kanto Kagaku, Japan. Luminol (product# 127-02581) and RB (product# 183-00122) were from FUJIFILM Wako Chemicals. NADH (product# 44327000) was from Oriental Yeast. Resazurin sodium salt (product# 191-07581) and resorufin (product# 73144) were from FUJIFILM Wako Chemicals and Sigma-Aldrich, USA. Acetate buffer (AB) was prepared by acetic acid (product# 017-00256, FUJIFILM Wako Chemicals) and sodium acetate (product# 192-01075, FUJIFILM Wako Chemicals). Phosphate buffer (PB) was made with potassium dihydrogen phosphate (product# 169-04245; FUJIFILM Wako Chemicals) and disodium hydrogen phosphate (product# 197-02865; FUJIFILM Wako Chemicals). Tris-HCl buffer (TB) was prepared by hydrochloric acid (product# 083-3485; FUJIFILM Wako Chemicals) and 2amino-2-hydroxymethyl-1,3-propanediol (product# 013-16385; FUJIFILM Wako Chemicals). Trisodium phosphate buffer (TPB) was prepared by potassium dihydrogen phosphate and trisodium phosphate dodecahydrate (product# 191-082885, FUJIFILM Wako Chemicals). All buffers made using ultrapure water prepared by PURELAB Flex (ELGA LabWater, U.K.).

### Comparison of detection method for target chemicals using red light

Figure 1A shows the measuring principle by target molecule by red light based on

luminol CL. Many oxidases consume oxygen to produce hydrogen peroxide when oxidizing the target molecule in the reaction. This hydrogen peroxide triggers luminol CL in the presence of luminol and HRP. Under normal conditions, luminol emission is blue with a central wavelength around 450–460 nm, but when RB is added to the reaction, energy transfer occurs, and RB FL (maximum wavelength around 590 nm) is emitted. Various other fluorophores can be used besides RB, but RB was selected based on its difference in peak wavelength from 400–500 nm. Fig. 1B shows a scheme for generating resorufin by triggering NADH produced by the reaction of NADH-dependent enzymes. It is possible to quantify the change in target molecule concentration using red light by resorufin FL (excitation 560 nm, emission 590 nm).

In the experiments, the optical wavelength spectra produced by each reaction were examined. In the case of luminol + RB, 1 mg of HRP and 1 mg of RB were dissolved in a luminol solution prepared at 5 mM using TB (at pH 10.1, 0.1 M). Hydrogen peroxide prepared to 10 mM was added to a cuvette containing this mixture and scanned for emission wavelength using a fluorescence spectrophotometer (product# F-7000, Hitachi High-Tech, Japan). Note that the cuvettes were shielded with a black cloth to avoid exposure to any excitation light. In the evaluation of an NADH-DP-resazurin system, resazurin was dissolved in PB (at pH 8.0, 0.1M) to prepare a 10 μM resazurin solution, and 1 mg of DP was added to prepare a resazurin-DP solution. Further 100 μM NADH solution was added, and FL spectra were obtained at an excitation wavelength of 560 nm.

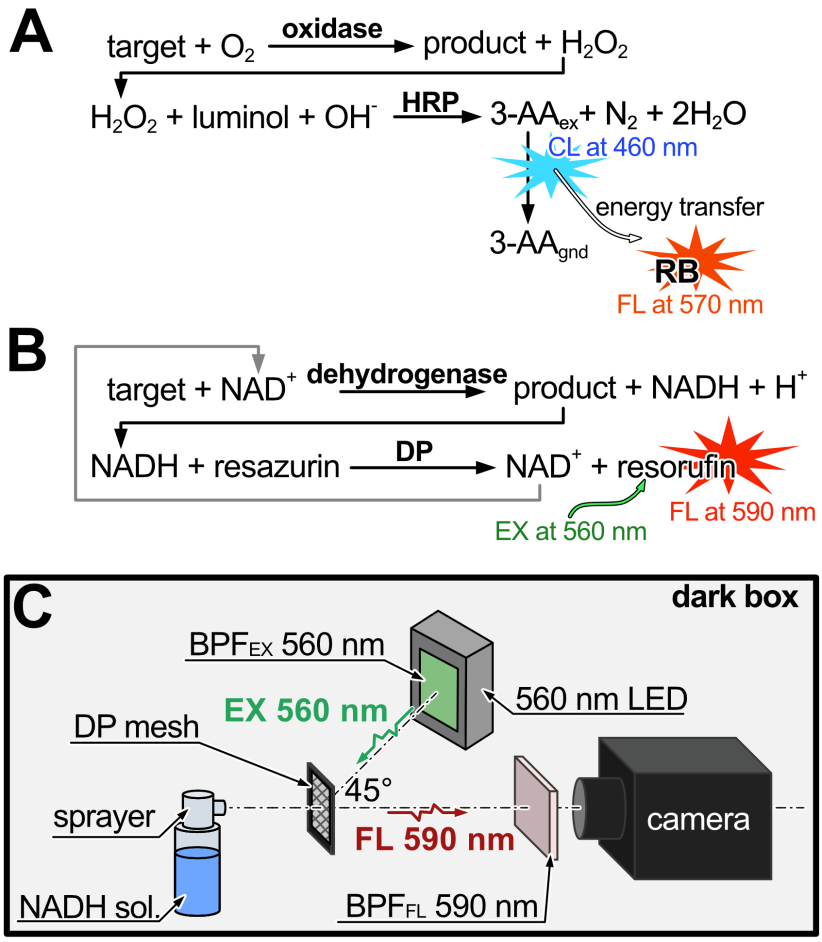


**Figure 1.** The target molecule detection method based on (A) luminol chemiluminescence and (B) NADH-mediated cascade reaction. The red light was used to detect molecule in both methods. (C) The setup for imaging of NADH in mist spray.

**Evaluation of dynamic ranges of NADH and resorufin using fluorescence macro imaging**

The same camera (product# C15550-20UP, Hamamatsu Photonics, Japan) was then used to acquire FL intensities emitted from various concentrations of NADH and resorufin to obtain the quantitative characteristics of each molecule. In the experiment, the optical system shown in Figs. S1A or S1B was used to observe NADH or resorufin, respectively. The NADH imaging system consisted of a ring-type UV-LED (custom-made, emission 340 nm, DOWA electronics, Japan) equipped with a bandpass filter (BPF, product#65-209, 492 ± 5 nm, Edmond optics, USA) for FL and a BPF (custom-made, 340 ± 42.5 nm, HOYA candeo optronics, Japan)

for excitation, as used in previous studies. An imaging target was placed at a distance of 60 mm from the lens. The resorufin imaging system consisted of a light source with five Yellow Green LEDs (product# 4903670676543, 550-570 nm, LED Generic, Japan), a BPF for excitation (product# HMZ0560, 560 ± 5 nm, Asahi Spectra, Japan), an imaging target, a BPF for FL (product# HMX0590, 590 ± 5 nm, Asahi Spectra, Japan), and a camera. All components were arranged on the same optical axis. In both imaging experiments, FL emitted from cotton mesh (product# 002-20377, 1.5 × 1.5 cm, Iwatsuki, Japan) soaked with 80 µL of NADH or resorufin solution prepared in PB (at pH 7.0, 0.1 M) was captured by the camera. The concentration of NADH or resorufin soaked in the cotton mesh was varied from 1 nM to 100 mM or 1 nM to 100 µM, respectively. Cotton mesh soaked with PB was also captured to obtain background images. The camera exposure time was set to 1 s for all experiments. The FL images were analyzed by using ImageJ2.[39] The entire area of the cotton mesh was set as the region of interest and the average intensity was calculated. Calibration curves were obtained by plotting the difference of average intensity between each concentration and background and curve fitting using Origin 2016.

**Optimization of reaction conditions of DP**

In the case of red-light imaging of NADH, DP was immobilized on cotton mesh, and DP-immobilized mesh was used in the experiment. For DP immobilization, first, 100 µM of PB (at pH 6.5, 0.1 M) containing 60 U/cm$^2$ DP was dropped onto a 1.5 × 1.5 cm cotton mesh and placed in a refrigerator for 1 h. Next, 18 µL of 2.5 v/v% GA (in PB at pH 7.0, 0.1 M) was added dropwise and placed in the refrigerator for 1.5 h. Finally, the DP-immobilized cotton mesh was rinsed with 300 µL of PB (at pH 6.5, 0.1 M). The prepared DP-immobilized mesh was placed in the optical system with 80 µL drops of 100 µM resazurin solution prepared in PB at pH 7.5 (see Fig. 1C). Excitation light was irradiated and 100 µM NADH solution was sprayed from

the back of the DP-immobilized mesh white camera took video. In displaying the distribution of FL intensity, the difference image between the images taken at the start of recording and those taken after that was calculated.

We then searched for optimal values for the buffer pH of the resazurin solution, the amount of DP used for immobilization, and the initial concentration of resazurin solution, which are expected to have a significant impact on the NADH quantification performance. For the selection of buffer pH, 100 μM of resazurin solutions were prepared using AB (at pH 4.0–6.0), PB (at pH 5.5–7.5), TB (at pH 7.5–9.0), and TPB (at pH 8.0–9.0). The prepared resazurin solution was soaked into a DP-immobilized mesh with 60 U/cm$^2$ DP. The output response was observed by spraying 50 μM NADH solution. Subsequently, DP-immobilized meshes with DP amounts of 0.6, 3, 6, 30, 60, and 100 U/cm$^2$ were soaked with 100 μM resazurin solution prepared in PB (at pH 6.5, 0.1 M) and sprayed with 50 μM NADH to determine DP amount for immobilization. Furthermore, the optimal initial resazurin concentration was examined by soaking the 60 U/cm$^2$ DP-immobilized mesh with 10, 30, 50, 100, 200, 300, and 1000 μM resazurin solution prepared in PB (at pH 6.5, 0.1 M) and spraying 50 μM NADH solution.

**Image analysis of dynamic changes of DP-mediated fluorescence**

Since the resorufin produced by the DP reaction remains after the reaction stops, it is impossible to know at what time to reaction occurred without observing all images. Therefore, we examined time-domain image differential analysis to calculate the DP reaction rate to observe the change in output in response to NADH spraying. In this section, FL images obtained by spraying 100 μM NADH onto 60 U/cm$^2$ DP-immobilized mesh soaked with 80 μL of 100 μM resazurin were analyzed in accordance with previous studies. First, background subtraction images were calculated. Then differential images were calculated using Equation (1).

$$\text{differential image} = \frac{\text{FL image}_i\text{-FL image}_{(\text{fps}\times\Delta t)}}{\Delta t} \quad (1)$$

Where $\Delta t = 10$, fps = 1, $i > 10$

**Quantitative characteristics for DP-mediated NADH image sensing**

NADH solutions from 1 nM to 100 μM were sprayed onto the DP-immobilized mesh using optimized conditions for red-light imaging of NADH. The resulting FL images and calculated differential images were used to evaluate the quantitative characteristic of NADH.

## Results and Discussions

**Spectral comparison for wavelength-based chemical imaging**

Figure 2A shows camera images of luminol CL and luminol CL + RB generated in cuvettes. These images show that luminol CL + RB has a visually different emission color than blue. The emission spectra of NADH FL, NADH-DP-resazurin (resorufin FL), luminol CL, and luminol CL + RB were normalized by the peak value of each spectrum and compared (see Fig. 2B). The results show that luminol CL and luminol CL + RB have a smaller difference in spectral shape compared to visual differences. The addition of RB reduced the light intensity around 420 nm and slightly sharpened the spectrum shape from 400–500 nm. In addition, a small and broad rise was observed around 600 nm. This spectral shape was considered to have a large overlap with NADH FL and luminol CL, which show blue light, making wavelength separation difficult during multiplexing measurements. In contrast, resorufin FL emitted via NADH-DP-resazurin system has a relatively sharp spectrum centered at 590 nm, with minimal overlap in the spectrum with the blue light at 400–500 nm. The shoulder around 560 nm was considered caused by the excitation light reaching the detector. As a result, the method using resorufin FL could be easily combined with luminol CL or NADH FL. In conclusion, we focused on the NADH-DP-resazurin system to investigate the possibility of chemical imaging

with red light.

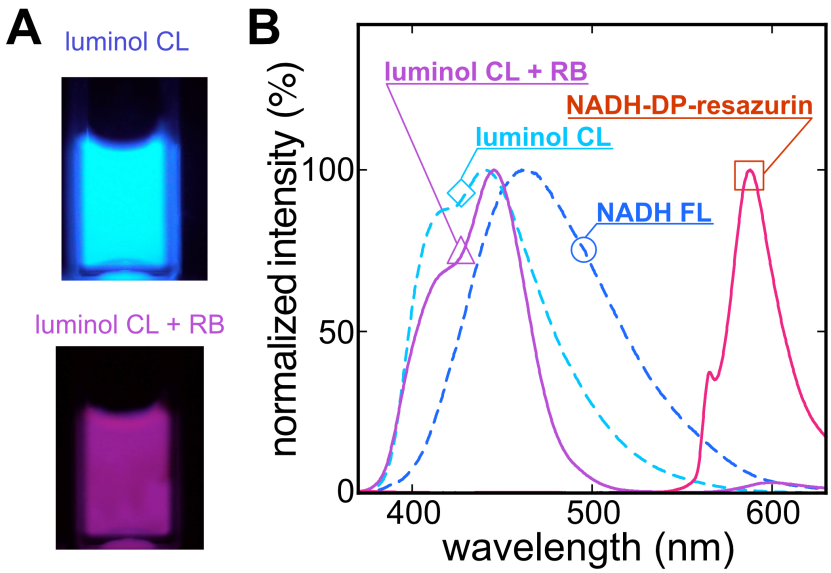


**Figure 2.** (A) photo images of luminol CL and luminol CL with RB, and (B) spectrum of (◇) luminol CL, (△) luminol CL + RB, (◯) NADH FL, and (□) DP-induced resorufin FL. All spectra were normalized by peak maximum intensity.

**Sensitivity of the system on NADH FL and resorufin FL**

Figures 3A and 3B show the results of microimaging of NADH FL and resorufin FL. The relationship between the average FL intensity of the acquired images and the concentrations of NADH and resorufin can be fitted by Equations (2) and (3) in the concentration ranges of 0.1–10000 μM and 0.03–300 μM, respectively. The limit of quantification (LoQ) calculated from the 10-fold value of the background standard deviation was 276 nM and 43 nM for NADH and resorufin, respectively. The NADH-DP-resorufin system requires an enzymatic reaction for the determination of NADH concentration. In general, the additional steps in a cascade reaction, lower the efficiency of the final product formation. Thus, the NADH-DP-resorufin system was expected to have lower detection sensitivity for NADH than the method using NADH FL directly for quantification. However, the sensitivity to resorufin was higher than that to NADH, suggesting that the effect of the enzymatic reaction on sensitivity may be counterbalancing.

This difference in detection sensitivity at low concentrations can be explained by FL quantum yield which is defined as the ratio of the number of photons emitted as FL to the number of photons absorbed. If the FL quantum yield is low, the FL intensity obtained will be low even if the same level of photoexcitation is possible. The absolute FL quantum yield of NADH in water is calculated to be 2.1%,28 while the FL quantum yield of resorufin was around 74%.[40]

$$\Delta\text{intensity (a.u.)} = A + \frac{B - A}{\left\{1 + \frac{[NADH\ conc.\ (\mu M)]^{-D}}{C}\right\}^{E}} \quad (2)$$

Where A = 6.540, B=2.502×$10^4$, C=1062, D = 0.9488, and E = 1.2743

$$\Delta\text{intensity (a.u.)} = A + \frac{B - A}{\left\{1 + \frac{[resorufin\ conc.\ (\mu M)]^{-D}}{C}\right\}^{E}} \quad (3)$$

Where A = 15.19, B=7291, C=25.38, D = 3.201, and E = 0.3022

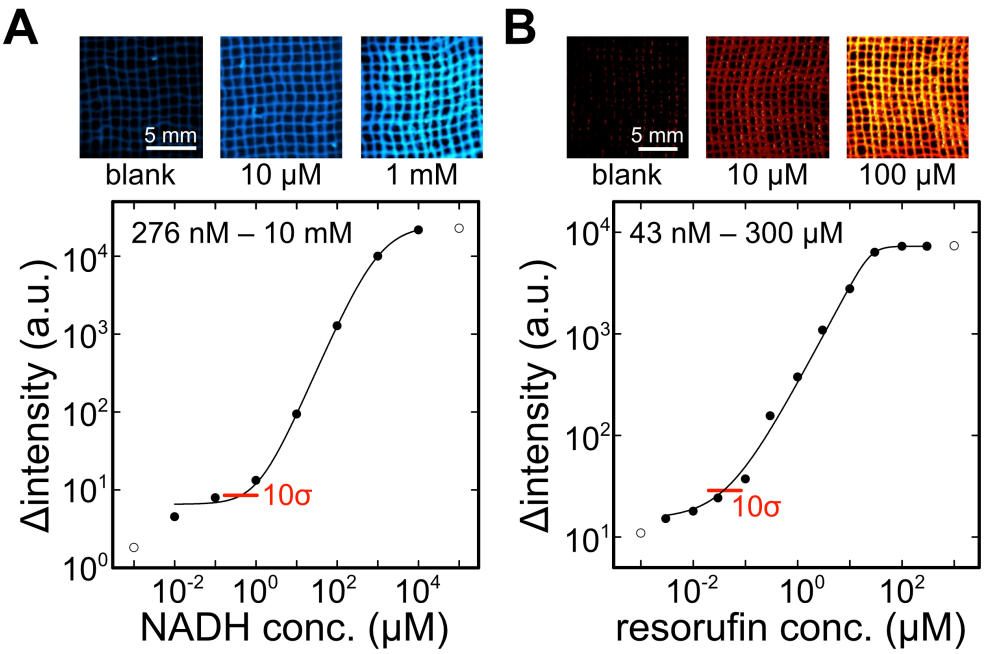


**Figure 3.** Results of image sensing of (A) NADH and (B) resorufin based on fluorescence

**Optimum conditions of buffer pH, immobilized amount, and initial resazurin concentration for NADH-DP-resazurin system**

Figure 4A shows the change over time in the FL intensity of resorufin produced when a resazurin-soaked DP-immobilized mesh was sprayed with NADH mist spray. The FL intensity of resorufin increased immediately after spraying, and it could be observed that the FL reached its equilibrium value. The difference between the baseline and equilibrium values was defined as ΔI, and the 90% response time (T90%) was calculated to be 31 s. Optimization of the NADH-DP-resazurin system was performed using ΔI as an indicator. The maximum value of ΔI was obtained at pH 6.5 among various buffer pH (response curve shown in Fig. S2A). The relationship between the amount of DP used for immobilization, ΔI, and T90% showed that the use of 60 U/cm2 DP was the best (see Fig. 4C, response curve shown in Fig. S2B). In addition, the effect of the initial resazurin concentration on ΔI was evaluated. As shown in Fig. 4D, a maximum value was observed at 100 μM, and higher additions resulted in a decrease in ΔI (response curve shown in Fig. S2C). Resazurin has high absorbance at 560 nm and 590 nm as shown in Figs. S3. Therefore, if a large amount of abundant resazurin remains after the reaction, excitation of resorufin is blocked by resazurin, and the resulting resorufin FL is also absorbed by resazurin. Based on the above experimental results, the reaction conditions for the NADH-DP-resazurin system were set to pH 6.5, DP amount 60 U/cm$^2$, and resazurin concentration 100 μM.

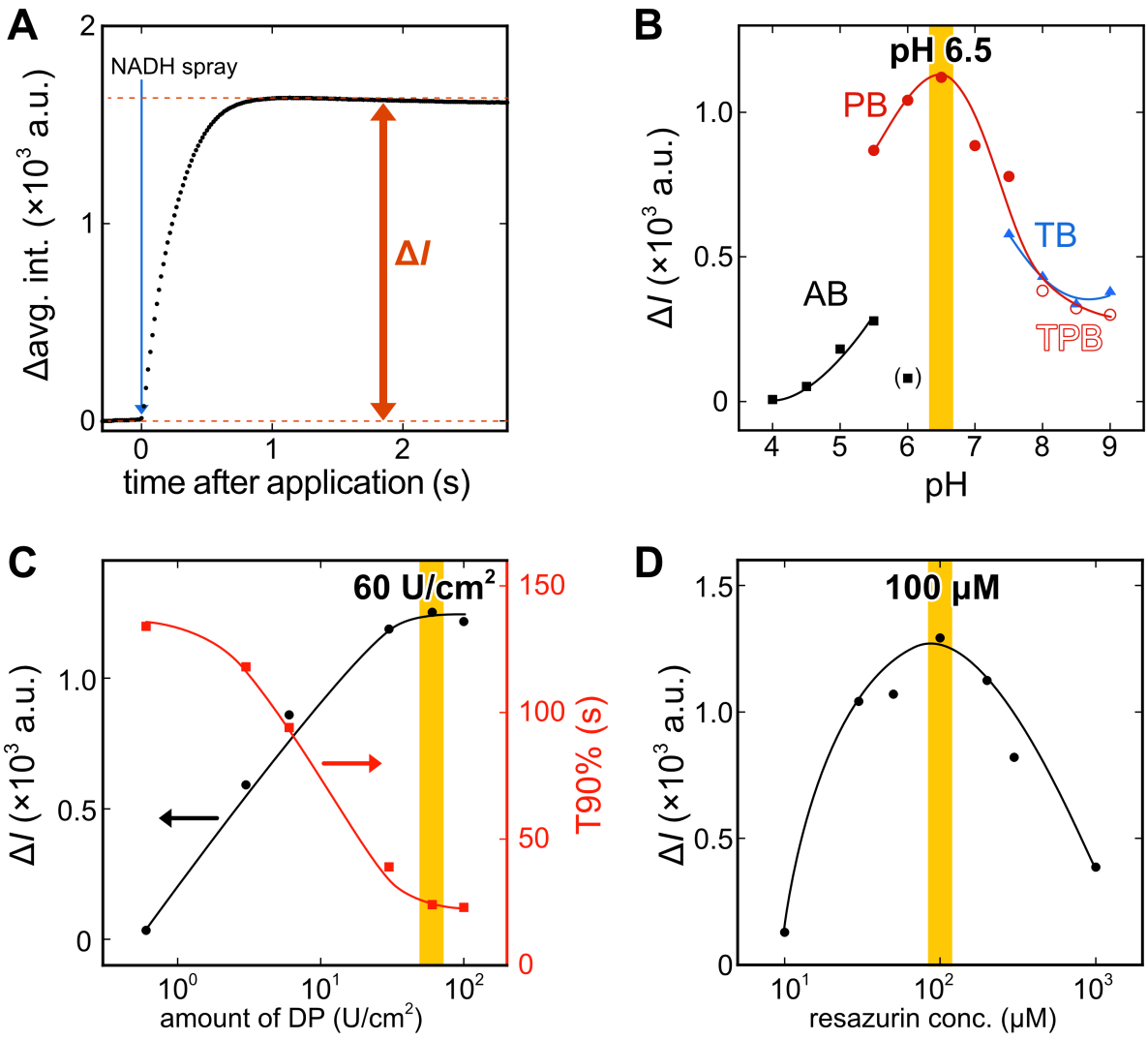


**Figure 4.** (A) Time course of the fluorescence change by applying NADH spray. (B) pH dependency of fluorescence change caused by applying NADH spray. (C) Relationship between the amount of DP used for immobilization. (D) Effect of initial resazurin concentration on $\Delta I$.

**Spatiotemporal imaging of NADH via DP-mediated resorufin FL**

Figure 5A shows FL images of resorufin on a DP-immobilized mesh produced by spraying NADH solution and a differential image (videos are shown in Supplemental Videos 1 and 2). By using differential analysis, it is easy to determine whether or not NADH currently being applied from the single frame as shown in these images. The numerical values of these

images showed that the T90% of peak ΔD is shorter than that of the FL intensity analysis (from 31 s to 10s).

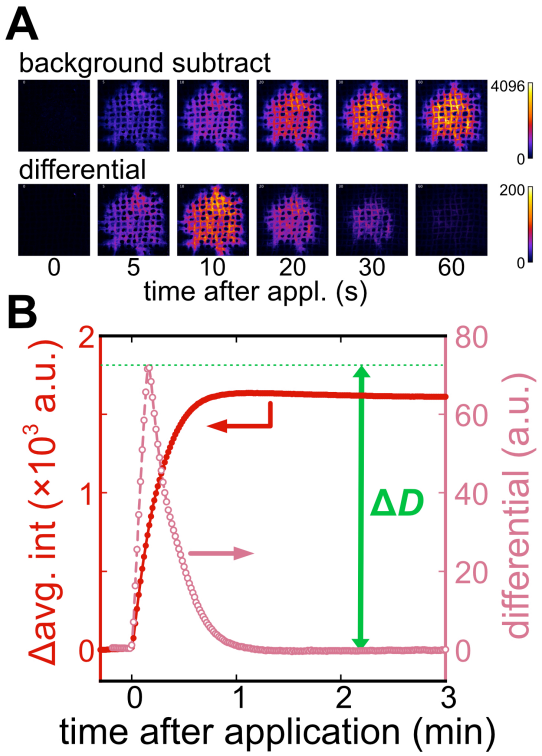


**Figure 5.** (A) Images of background subtract FL and differential analysis (B) Time course of fluorescence changes and differential value.

**Quantitative characteristics of NADH by using DP-mediated resorufin FL**

Figures 6A and 6B show the changes over time of resorufin FL intensity and the differential value obtained by spraying different concentrations of NADH on DP-immobilized meshes under optimal conditions. The FL intensity exhibited equilibrium values that carried with the concentration of NADH, and ΔD changed accordingly. NADH calibration curves were calculated from the obtained ΔI and ΔD, which could be fitted by Equations (4) and (5) in the concentration range of 0.01–100 μM, respectively. The LoQs were 0.7 and 2.7 μM for ΔI and ΔD, respectively. These LoQs were 2.5- and 9.6-fold higher than those obtained when NADH itself was excited (0.28 μM) taken by the same camera, indicating that the sensitivity was reduced by the enzymatic reaction, which was mentioned earlier. On the other hand, the LoQ

of NADH in the previous systems we have reported was tens of μM (using a UV-LED sheet array and a HEED-HARP camera) and hundreds of nM (using a ring-type UV-LED and a CMOS RGB camera). This suggests that the optical system and NADH-DP-resazurin system developed in this study can be applied to VOC imaging by red light in combination with other NADH-dependent enzymes.

$$\Delta I(\text{a.u.}) = A + B \times [NADH\ conc.(\mu M)]^C \quad (3)$$

Where A = 14.798, B=51.061, C=0.81505

$$\Delta D(\text{a.u.}) = A + B \times [NADH\ conc.(\mu M)]^C \quad (3)$$

Where A = 4.5013, B=3.7908, C=0.86115

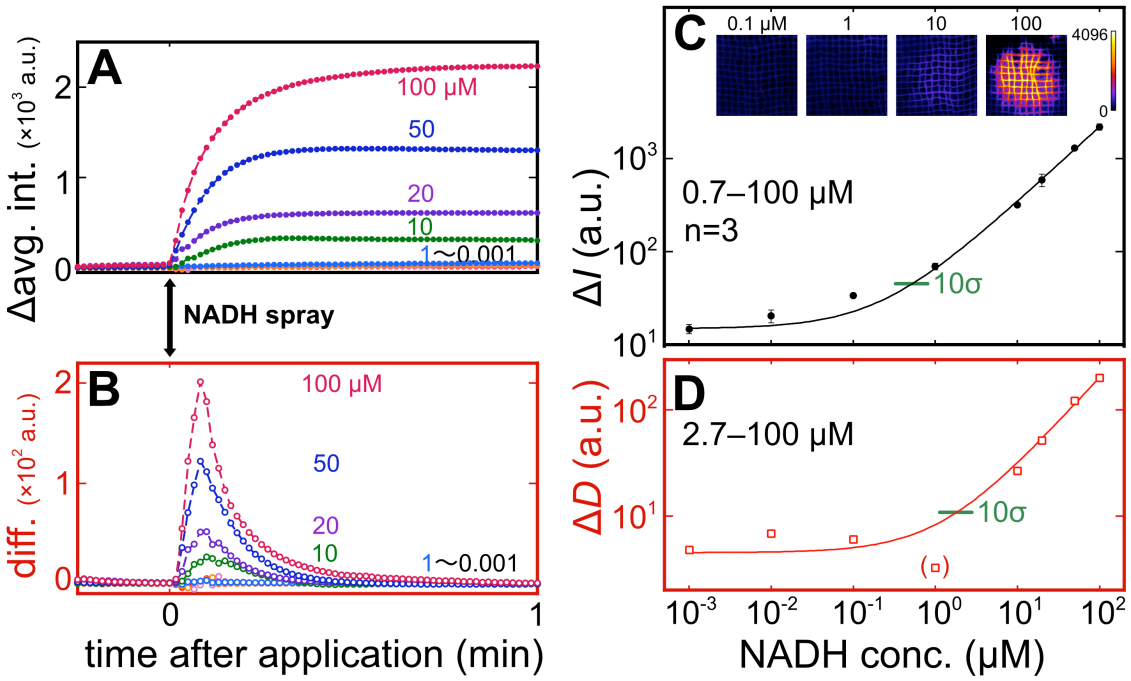


**Figure 6.** Response curves of (A) FL change and (B) its differential with different concentration of NADH. Calibration curve for the NADH concentration based on (C) $\Delta I$ and (D) $\Delta D$.

## Conclusion

In this study, we investigated the methodology of chemical imaging with red light to achieve multiplexing with blue light, which is frequently used in enzymatic optical biosensors.

The suitability of luminol CL + RB and NADH-DP-resazurin system as candidates for the use of red light for quantitative imaging of hydrogen peroxide or NADH was evaluated. The results showed that resorufin, an FL molecule produced by the NADH-DP-resazurin system, has a minimal wavelength overlap with luminol CL and NADH FL. Therefore, we optimized the reaction conditions of the NADH-DP-resazurin system and found that the detection sensitivity of NADH was maximized by using a 100 μM resazurin solution prepared with PB at pH 6.5 for 60 U/cm$^2$ DP-immobilized on a cotton mesh. Spatiotemporal imaging of resorufin produced by the NADH-DP-resazurin system was also achieved by time-domain image differential and a good response was observed (T90% = 10 s). The LoQ of NADH by using the NADH-DP-resazurin system was 0.7 and 2.7 μM based on FL intensity and reaction rate, respectively. Those LoQs were comparable to the LoQ of NADH of our previous system for VOC imaging using NADH-dependent enzymes. In the future, this system will be combined with NADH-dependent enzymes for red fluorescence VOC imaging and multiplexed with a blue fluorescence VOC imaging method to be applied for same-space imaging of multiple VOCs at the same time.

## Supporting information

The supporting Information is available free of charge at XXX.

Additional figures: **Figure S1.** Response curves of the base system against standard acetone gas; **Figure S2.** Typical response curves in evaluations of (A) buffer pH, (b) amount of DP for immobilization, (C) concentration of initial resazurin; **Figure S3.** Absorption spectrum of resazurin at different concentrations. (PDF)

**Supplemental Video 1.** 30-times fast forward moving images of FL generated on DP-immobilized mesh by applying NADH mist spray.

**Supplemental Video 2.** 30-times fast forward moving images of results of time-domain image differential analysis on FL images of Supplemental Video 1.

## Notes

The authors declare that they have no known competing financial interests or personal relationships that could have appeared to influence the work reported in this paper.

## Acknowledgments

This work was supported by the Japan Society for the Promotion of Science (JSPS) KAKENHI Grant Numbers JP21H04888, JP22K18416, and JP23H03864, JST ACT-X Grant Number JPMJAX23K2, the Cooperative Research Project of Research Center for Biomedical Engineering.

## References


(1) Lawal, O.; Ahmed, W. M.; Nijsen, T. M. E.; Goodacre, R.; Fowler, S. J. Exhaled Breath Analysis: A Review of 'Breath-Taking' Methods for off-Line Analysis. *Metabolomics* **2017**, *13* (10), 110. https://doi.org/10.1007/s11306-017-1241-8.

(2) S., K.; Saquib, M.; Poojary, H.; Illanad, G.; Valavan, D.; M, S.; Nayak, R.; Mazumder, N.; Ghosh, C. Skin Emitted Volatiles Analysis for Noninvasive Diagnosis: The Current Advances in Sample Preparation Techniques for Biomedical Application. *RSC Adv.* **2024**, *14* (17), 12009–12020. https://doi.org/10.1039/D4RA01579G.

(3) Shirasu, M.; Touhara, K. The Scent of Disease: Volatile Organic Compounds of the Human Body Related to Disease and Disorder. *J. Biochem. (Tokyo)* **2011**, *150* (3), 257–266. https://doi.org/10.1093/jb/mvr090.

(4) *Volatile Biomarkers: Non-Invasive Diagnosis in Physiology and Medicine*, 1st ed.; Amann, A., Smith, D., Eds.; Elsevier: Amsterdam ; Boston, 2013.

(5) Davies, S. J.; Španěl, P.; Smith, D. Breath Analysis of Ammonia, Volatile Organic Compounds and Deuterated Water Vapor in Chronic Kidney Disease and during Dialysis. *Bioanalysis* **2014**, *6* (6), 843–857. https://doi.org/10.4155/bio.14.26.

(6) Güntner, A. T.; Weber, I. C.; Schon, S.; Pratsinis, S. E.; Gerber, P. A. Monitoring Rapid Metabolic Changes in Health and Type-1 Diabetes with Breath Acetone Sensors. *Sens. Actuators B Chem.* **2022**, *367*, 132182. https://doi.org/10.1016/j.snb.2022.132182.

(7) Chen, X.; Zhang, K.; Yin, Z.; Fang, M.; Pu, W.; Liu, Z.; Li, L.; Sinues, P.; Dallmann, R.; Zhou, Z.; Li, X. Online Real-Time Monitoring of Exhaled Breath Particles Reveals Unnoticed Transport of Nonvolatile Drugs from Blood to Breath. *Anal. Chem.* **2021**, *93* (12), 5005–5008. https://doi.org/10.1021/acs.analchem.1c00509.

(8) Drabińska, N.; Flynn, C.; Ratcliffe, N.; Belluomo, I.; Myridakis, A.; Gould, O.; Fois, M.; Smart, A.; Devine, T.; Costello, B. D. L. A Literature Survey of All Volatiles from Healthy Human Breath and Bodily Fluids: The Human Volatilome. *J. Breath Res.* **2021**, *15* (3), 034001. https://doi.org/10.1088/1752-7163/abf1d0.

(9) Majchrzak, T.; Wojnowski, W.; Lubinska-Szczygeł, M.; Różańska, A.; Namieśnik, J.; Dymerski, T. PTR-MS and GC-MS as Complementary Techniques for Analysis of Volatiles: A Tutorial Review. *Anal. Chim. Acta* **2018**, *1035*, 1–13. https://doi.org/10.1016/j.aca.2018.06.056.

(10) Smith, D.; Španěl, P.; Demarais, N.; Langford, V. S.; McEwan, M. J. Recent Developments and Applications of Selected Ion Flow Tube Mass Spectrometry (SIFT-MS). *Mass Spectrom. Rev.* **2023**, e21835. https://doi.org/10.1002/mas.21835.

(11) Zhao, Y.; Liu, Y.; Han, B.; Wang, M.; Wang, Q.; Zhang, Y. Fiber Optic Volatile Organic Compound Gas Sensors: A Review. *Coord. Chem. Rev.* **2023**, *493*, 215297. https://doi.org/10.1016/j.ccr.2023.215297.

(12) Wang, L. Metal-Organic Frameworks for QCM-Based Gas Sensors: A Review. *Sens. Actuators Phys.* **2020**, *307*, 111984. https://doi.org/10.1016/j.sna.2020.111984.

(13) Shinde, P. V.; Rout, C. S. Magnetic Gas Sensing: Working Principles and Recent Developments. *Nanoscale Adv.* **2021**, *3* (6), 1551–1568. https://doi.org/10.1039/D0NA00826E.

(14) Minami, K.; Imamura, G.; Tamura, R.; Shiba, K.; Yoshikawa, G. Recent Advances in Nanomechanical Membrane-Type Surface Stress Sensors towards Artificial Olfaction. *Biosensors* **2022**, *12* (9), 762. https://doi.org/10.3390/bios12090762.

(15) Jha, R. K. Non-Dispersive Infrared Gas Sensing Technology: A Review. *IEEE Sens. J.* **2022**, *22* (1), 6–15. https://doi.org/10.1109/JSEN.2021.3130034.

(16) Gardner, E. L. W.; Gardner, J. W.; Udrea, F. Micromachined Thermal Gas Sensors—A Review. *Sensors* **2023**, *23* (2), 681. https://doi.org/10.3390/s23020681.

(17) Gaggiotti, S.; Della Pelle, F.; Mascini, M.; Cichelli, A.; Compagnone, D. Peptides, DNA and MIPs in Gas Sensing. From the Realization of the Sensors to Sample Analysis. *Sensors* **2020**, *20* (16), 4433. https://doi.org/10.3390/s20164433.
(18) Dey, A. Semiconductor Metal Oxide Gas Sensors: A Review. *Mater. Sci. Eng. B* **2018**, *229*, 206–217. https://doi.org/10.1016/j.mseb.2017.12.036.
(19) Chowdhury, N. K.; Bhowmik, B. Micro/Nanostructured Gas Sensors: The Physics behind the Nanostructure Growth, Sensing and Selectivity Mechanisms. *Nanoscale Adv.* **2021**, *3* (1), 73–93. https://doi.org/10.1039/D0NA00552E.
(20) Benhaddouch, T. E.; Pinzon, S. K.; Landi, D. M. C.; Marcial, J.; Mehta, P.; Romero, K.; Rockward, T.; Bhansali, S.; Dong, D. Review—Micro-Fuel Cell Principal Biosensors for Monitoring Transdermal Volatile Organic Compounds in Humans. *ECS Sens. Plus* **2022**, *1* (4), 041602. https://doi.org/10.1149/2754-2726/aca95b.
(21) Amiri, V.; Roshan, H.; Mirzaei, A.; Neri, G.; Ayesh, A. I. Nanostructured Metal Oxide-Based Acetone Gas Sensors: A Review. *Sensors* **2020**, *20* (11), 3096. https://doi.org/10.3390/s20113096.
(22) Arakawa, T.; Iitani, K.; Toma, K.; Mitsubayashi, K. Biosensors: Gas Sensors. In *Encyclopedia of Sensors and Biosensors (First Edition)*; Narayan, R., Ed.; Elsevier: Oxford, 2023; pp 478–504. https://doi.org/10.1016/B978-0-12-822548-6.00066-2.
(23) Mitsubayashi, K.; Toma, K.; Iitani, K.; Arakawa, T. Gas-Phase Biosensors: A Review. *Sens. Actuators B Chem.* **2022**, *367*, 132053. https://doi.org/10.1016/j.snb.2022.132053.
(24) Schäferling, M. The Art of Fluorescence Imaging with Chemical Sensors. *Angew. Chem. Int. Ed.* **2012**, *51* (15), 3532–3554. https://doi.org/10.1002/anie.201105459.
(25) Weckhuysen, B. M. Chemical Imaging of Spatial Heterogeneities in Catalytic Solids at Different Length and Time Scales. *Angew. Chem. Int. Ed.* **2009**, *48* (27), 4910–4943. https://doi.org/10.1002/anie.200900339.
(26) Iitani, K.; Toma, K.; Arakawa, T.; Mitsubayashi, K. Transcutaneous Blood VOC Imaging System (Skin-Gas Cam) with Real-Time Bio-Fluorometric Device on Rounded Skin Surface. *ACS Sens.* **2020**, *5* (2), 338–345. https://doi.org/10.1021/acssensors.9b01658.
(27) Iitani, K.; Ichikawa, K.; Toma, K.; Arakawa, T.; Mitsubayashi, K. Biofluorometric Gas-Imaging System for Evaluating the Ripening Stages of “La France” Pear Based on Ethanol Vapor Emitted via the Epicarp. *ACS Sens.* **2024**.
(28) Wang, Y. W.; Reder, N. P.; Kang, S.; Glaser, A. K.; Liu, J. T. C. Multiplexed Optical Imaging of Tumor-Directed Nanoparticles: A Review of Imaging Systems and Approaches. *Nanotheranostics* **2017**, *1* (4), 369–388. https://doi.org/10.7150/ntno.21136.
(29) Lee, H.; Kim, J.; Kim, H.-H.; Kim, C.-S.; Kim, J. Review on Optical Imaging Techniques for Multispectral Analysis of Nanomaterials. *Nanotheranostics* **2022**, *6* (1), 50–61. https://doi.org/10.7150/ntno.63222.
(30) Chen, K.; Li, W.; Xu, K. Super-Multiplexing Excitation Spectral Microscopy with Multiple Fluorescence Bands. *Biomed. Opt. Express* **2022**, *13* (11), 6048. https://doi.org/10.1364/BOE.473241.
(31) Blum, L. J.; Marquette, C. A. CHEMILUMINESCENCE-BASED SENSORS. In *Optical Chemical Sensors*; Baldini, F., Chester, A. N., Homola, J., Martellucci, S., Eds.; Springer Netherlands: Dordrecht, 2006; pp 157–178. https://doi.org/10.1007/1-4020-4611-1_8.
(32) Zhou, Y.; Xu, Z.; Yoon, J. Fluorescent and Colorimetric Chemosensors for Detection of Nucleotides, FAD and NADH: Highlighted Research during 2004–2010. *Chem. Soc. Rev.* **2011**, *40* (5), 2222. https://doi.org/10.1039/c0cs00169d.

(33) Sun, P.; Zhang, H.; Sun, Y.; Liu, J. The Recent Development of Fluorescent Probes for the Detection of NADH and NADPH in Living Cells and in Vivo. *Spectrochim. Acta. A. Mol. Biomol. Spectrosc.* **2021**, *245*, 118919. https://doi.org/10.1016/j.saa.2020.118919.

(34) Park, S. Y.; Yoon, S. A.; Cha, Y.; Lee, M. H. Recent Advances in Fluorescent Probes for Cellular Antioxidants: Detection of NADH, hNQO1, H2S, and Other Redox Biomolecules. *Coord. Chem. Rev.* **2021**, *428*, 213613. https://doi.org/10.1016/j.ccr.2020.213613.

(35) Candeias, L. P.; MacFarlane, D. P. S.; McWhinnie, S. L. W.; Maidwell, N. L.; Roeschlaub, C. A.; Sammes, P. G.; Whittlesey, R. The Catalysed NADH Reduction of Resazurin to Resorufin. *J. Chem. Soc. Perkin Trans. 2* **1998**, No. 11, 2333–2334. https://doi.org/10.1039/a806431h.

(36) Hall, M. D.; Simeonov, A.; Davis, M. I. Avoiding Fluorescence Assay Interference—The Case for Diaphorase. *ASSAY Drug Dev. Technol.* **2016**, *14* (3), 175–179. https://doi.org/10.1089/adt.2016.707.

(37) Navas Díaz, A.; González García, J. A.; Lovillo, J. Enhancer Effect of Fluorescein on the Luminol-H2O2-Horseradish Peroxidase Chemiluminescence: Energy Transfer Process. *J. Biolumin. Chemilumin.* **1997**, *12* (4), 199–205. https://doi.org/10.1002/(SICI)1099-1271(199707/08)12:4<199::AID-BIO445>3.0.CO;2-U.

(38) Zhou, Y.; Du, J.; Wang, Z. Fluorescein and Its Derivatives: New Coreactants for Luminol Chemiluminescence Reaction and Its Application for Sensitive Detection of Cobalt Ion. *Talanta* **2019**, *191*, 422–427. https://doi.org/10.1016/j.talanta.2018.09.007.

(39) Rueden, C. T.; Schindelin, J.; Hiner, M. C.; DeZonia, B. E.; Walter, A. E.; Arena, E. T.; Eliceiri, K. W. ImageJ2: ImageJ for the next Generation of Scientific Image Data. *BMC Bioinformatics* **2017**, *18* (1), 529. https://doi.org/10.1186/s12859-017-1934-z.

(40) Bueno, C.; Villegas, M. L.; Bertolotti, S. G.; Previtali, C. M.; Neumann, M. G.; Encinas, M. V. The Excited-State Interaction of Resazurin and Resorufin with Aminesin Aqueous Solutions. Photophysics and Photochemical Reaction. *Photochem. Photobiol.* **2002**, *76* (4), 385–390. https://doi.org/10.1562/0031-8655(2002)0760385TESIOR2.0.CO2.

479 **TOC only**

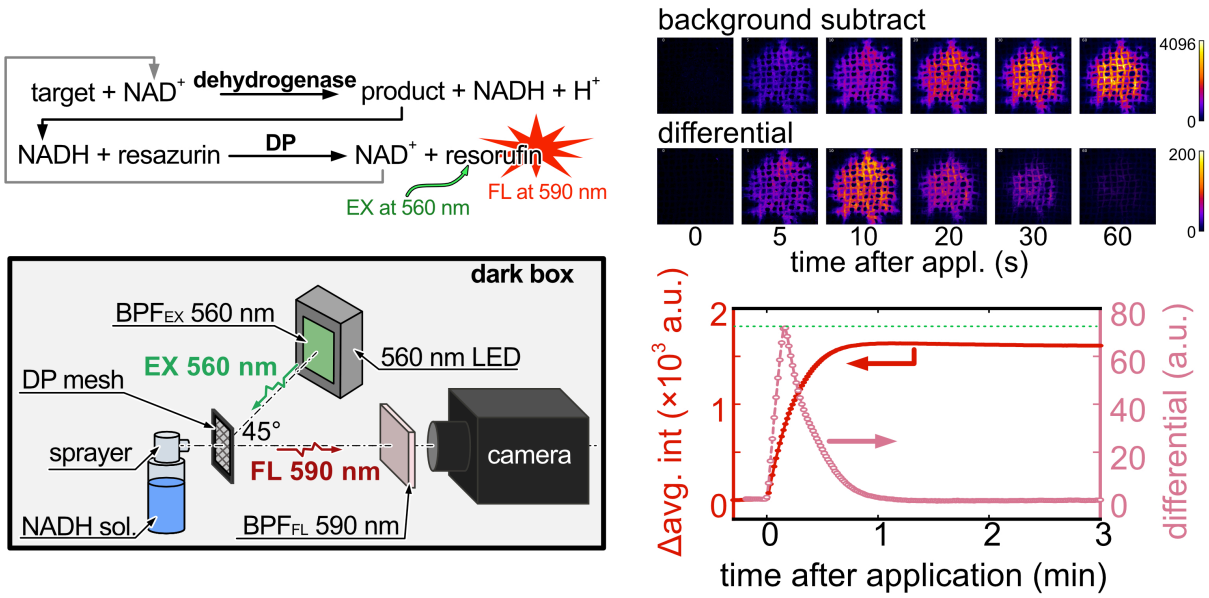


480